

Article

Hybrid-Compliant System for Soft Capture of Uncooperative Space Debris

Maxime Hubert Delisle ^{*,†} , Olga-Orsalia Christidi-Loumpasefski [†], Barış C. Yalçın, Xiao Li, Miguel Olivares-Mendez and Carol Martinez 

Space Robotics Research Group, SnT Interdisciplinary Centre for Security, Reliability and Trust, University of Luxembourg, 6 Rue Richard Coudenhove-Kalergi, 1359 Luxembourg, Luxembourg; miguel.olivaresmendez@uni.lu (M.O.-M.)

* Correspondence: maxime.hubertdelisle@uni.lu

† These authors contributed equally to this work.

Featured Application: The proposed hybrid-compliant concept is meant to be part of a space debris capture system.

Abstract: Active debris removal (ADR) is positioned by space agencies as an in-orbit task of great importance for stabilizing the exponential growth of space debris. Most of the already developed capturing systems are designed for large specific cooperative satellites, which leads to expensive one-to-one solutions. This paper proposed a versatile hybrid-compliant mechanism to target a vast range of small uncooperative space debris in low Earth orbit (LEO), enabling a profitable one-to-many solution. The system is custom-built to fit into a CubeSat. It incorporates active (with linear actuators and impedance controller) and passive (with revolutive joints) compliance to dissipate the impact energy, ensure sufficient contact time, and successfully help capture a broader range of space debris. A simulation study was conducted to evaluate and validate the necessity of integrating hybrid compliance into the ADR system. This study found the relationships among the debris mass, the system's stiffness, and the contact time and provided the required data for tuning the impedance controller (IC) gains. This study also demonstrated the importance of hybrid compliance to guarantee the safe and reliable capture of a broader range of space debris.

Keywords: space debris; active debris removal; impedance controller; in-orbit servicing; uncooperative satellites; gecko-inspired dry adhesive



Citation: Hubert Delisle, M.; Christidi-Loumpasefski, O.-O.; Yalçın, B.C.; Li, X.; Olivares-Mendez, M.; Martinez, C. Hybrid-Compliant System for Soft Capture of Uncooperative Space Debris. *Appl. Sci.* **2023**, *13*, 7968. <https://doi.org/10.3390/app13137968>

Academic Editors: Lorenzo Olivieri, Kanjuro Makihara and Leonardo Barilaro

Received: 30 May 2023

Revised: 28 June 2023

Accepted: 3 July 2023

Published: 7 July 2023



Copyright: © 2023 by the authors. Licensee MDPI, Basel, Switzerland. This article is an open access article distributed under the terms and conditions of the Creative Commons Attribution (CC BY) license (<https://creativecommons.org/licenses/by/4.0/>).

1. Introduction

Since humankind initiated space activities more than 60 years ago, the number of in-orbit objects has increased [1]. More than 330 million debris objects not bigger than 1 cm are in orbit. The number of objects between 1 and 10 cm is close to 1 million, whereas there are around 36,500 debris objects greater than 10 cm [2]. The Kessler Syndrome states that the amount of space debris is growing exponentially [3], which leads to a crucial problem for ongoing and future space missions. Two approaches have been proposed to mitigate the space debris problem—active debris removal (ADR) and passive debris removal (PDR). However, PDR cannot achieve the desired stabilized number of debris in the foreseeable future. Even if space launches stop, the number of space debris would still increase due to future collisions. Therefore, ADR is required [4].

The problem with space debris is that most targets are not designed for removal. They are uncooperative for capturing [5] and they do not include specific grippers, handles, or markers to make capturing easier [6]. Additionally, each debris object has a unique geometry, velocity, and material [7]. The fact that they can be tumbling at hyper-velocity constitutes a crucial danger at any orbit [8]. Hence, capturing autonomously and harmlessly uncooperative objects demands reliability, robustness, and control at the impact,

as the space environment and the crucial nature of the mission are demanding. These requirements give the capturing phase the most critical role in the mission.

Capturing mechanisms can interact differently with the debris; an Energy-Transfer Classification (ET-Class) was proposed in [9]. For instance, the *Impact Energy Dissipation (ET2)* class implies a capture with a decrease of energy at the first impact. In this class, the rigid and flexible capturing methods stand out as the most promising for their reliability. The rigid capturing operation was one of the first capturing methods tried for the realization of mechanical contact in space. However, this method requires, in some cases, extremely expensive motion control since any misalignment during the contact can push the debris far away [10,11], especially if the object is tumbling at high velocity [12]. Additionally, any rigid capturing mechanism must be lightweight and compatible with different space debris volumes [13]. As a result, the rigid capturing method is more applicable for cooperative targets that have proper docking ports [14].

In the literature, many rigid robotic structures are from single-arm to multiple-arms [15,16]. Multiple arms are controlled by more complex control algorithms, such as sliding mode control or adaptive control [17]. For single-arm rigid capturing methods, the classical PID control approach is enough to achieve position and velocity control of the end-effector [18]. Nowadays, reinforcement learning (RL)- [19,20], model predictive control (MPC)- [21], and \mathcal{H}_∞ -based [22] methods are also researched. Yet, the most crucial problem regarding rigid capturing methods remains the same, which is the difficulty of achieving robust mechanical interaction using rigid structures in space, since rigidity lacks appropriate impact energy dissipation in a frictionless environment. Therefore, both academic and industrial research are inclined to focus on flexible capturing methods rather than rigid capturing methods [23]. Regarding flexible capturing methods, shape memory alloys (SMA) and pneumatic capturing mechanisms are nowadays part of the most popular flexible mechanisms [24–26]. They can be categorized in the *ET2* category, as capturing mechanisms of this class decrease the impact energy of the debris at the very first contact, according to the ET-Class. For example, capturing mechanisms using SMA material can fully comply with the debris geometry. Moreover, the actuation of SMA does not demand high energy consumption [27,28]. The most sophisticated study accomplished in this field is MEDUSA. MEDUSA has flexible arms actuated by electrical inputs that can grasp nearly any object. When a simple electrical signal triggers the nitinol wires, the arms of MEDUSA begin to adapt their shape and grasp space debris [29]. Many detailed experiments showed the great robustness of the mechanical contact. However, despite promising on-ground facility results, these capturing methods have not been tested in space yet, making their performance fuzzy for on-site space applications.

In addition, more flexible mechanisms take advantage of the gecko-inspired dry adhesive to stick to the debris surface. However, they are, so far, either not suitable for small autonomous integration applications [30] or fitting a specific debris shape [31,32]. Moreover, a critical factor for a capturing system is its ability to absorb the first impact with the target; a strong and rigid impact can lead to mechanical failure and, thus, to mission failure or debris generation. To deal with this, researchers have integrated either passive [33] or active [34] compliance into their systems. However, to ensure adequate contact time with the debris for the adhesive to stick to the debris surface during the impact, passive compliance, although essential to dissipate the impact energy, is not enough; controlled active compliance of the interaction is required [35]. To the authors' knowledge, no such hybrid system, i.e., a system with both active and passive compliance, has yet been proposed.

Therefore, this paper proposes the following:

- A concept for an active debris removal capturing phase (Section 2);
- A hybrid-compliant system for the soft capture of space debris (Section 3);
- An impedance control design for the proposed hybrid-compliant system (Section 4).

The proposed flexible, versatile hybrid-compliant system of class *ET2* [9], custom-built to fit a CubeSat, is displayed in Figure 1. This new system targets a vast range of small debris, enabling a profitable one-to-many solution. In contrast to previous concepts,

the mechanism's compliance is hybrid. It incorporates active (with linear actuators and impedance controller) and passive (thanks to revolute joints) compliance to dissipate the impact energy, allow adequate contact time, and successfully help capture a broader range of space debris.



Figure 1. Concept of a CubeSat-based system for capturing small debris.

Impedance control (IC) is an example of active interaction control, incorporating lumped parameters [36]. For a mechanism in contact with debris, IC can regulate the relationship between the mechanism's tip position and the impact force [37,38]. An essential part of IC is the proper tuning of its gains. By adjusting them regarding the mass of the debris to be captured, the capturing system can target a wider range of debris. In this paper, a simulation study was conducted. It presented the correlation between the debris mass, the ADR system's hybrid compliance, and the contact time, providing the required data for appropriate IC gains tuning. In addition, the necessity of hybrid compliance and the IC was validated.

This paper is organized as follows. Section 2 introduces the space debris capture problem with a brief on space environment statistics, focusing on LEOs to determine which shape is the most common and must be targeted first. Additionally, the section presents the proposed concept of operations (ConOps) for an ADR Capturing Phase. Section 3 presents the proposed hybrid-compliant system, and its integration into the proposed capturing phase is described. Section 4 introduces the impedance controller, a critical component of the proposed hybrid-compliant system. Finally, Section 5 presents the simulation study and discussion of the results, and Section 6 presents the conclusions and direction of future work.

2. Space Debris Capture

Despite the growing concern about space debris, no autonomous capturing system has been officially used yet. The required technologies can be quite diverse and by 2025 we will see the launch of the first autonomous chaser satellites by ClearSpace to remove an ESA-owned item from orbit (ClearSpace-1 mission [39,40]).

ADR missions depend a lot on the targeted debris. The most commonly studied solution is to design one capturing system for one specific debris (one-to-one solution). Currently, voluminous and well-known satellites are the ones aimed to be targeted first. However, although these satellites are one of the main threats to generating more space debris, it is only one side of the problem. The new mega-constellations of CubeSats coming in the next decade in LEO (around the 500–700 km orbits) will increase the number of decommissioned satellites remaining in orbit. As a result, the urge to tackle the small satellites in LEO is and will be real.

The capturing mechanism plays a key role in the success of an autonomous space debris removal mission, especially if it is designed to target a wide range of debris, as the one proposed in this paper. To that extent, to design such a system, it is of utmost

importance to know about the variety of objects in LEO, obtain knowledge of that data, and determine what range of debris our mechanism should target first. These parameters will impact the design of an autonomous ADR system.

2.1. Debris Data

Space environment statistics is a new space debris topic addressing debris tracking. Due to the technological limitations of the surveillance networks, small-size debris is currently not trackable. In December 2022, more than 32,500 objects were regularly tracked by space surveillance networks. In contrast, more than 130 million objects starting from 1 mm in size are estimated to be in space orbit, based on statistical models [2]. The growing space debris issue in LEO creates the need for knowledge about those objects to design adequate debris removal systems. As ESA made available the catalogue of the tracked objects via the single-source DISCOS (Database and Information System Characterising Objects in Space) dataset [41], which is updated every few months, it is possible to analyze the LEO debris population. DISCOS plays a daily role in some of the ESA activities, such as collision avoidance, re-entry analyses, and for contingency support.

By analyzing the DISCOS dataset, a debris population of almost 20,000 objects with nearly 300 different shapes was found in LEO. For each object, the available features are their mass, shape (with size characteristics, when available), and information about their orbits (apogee, perigee). All these objects could potentially threaten any space mission. However, we prioritize the shapes more commonly found in LEO (found more than a hundred times) for designing our capturing mechanism. Additionally, as the focus is on small satellite removal, the targeted debris' size and mass are non-negligible factors. To that extent, we narrowed down the catalogue of objects in LEO to those lower than or equal to 100 kg.

The total number of objects found in LEO with the mentioned parameters was 4162. Among the 107 different specific shapes left, Sphere, Box, Box + 2 Pan (box shape with two solar panels), Cyl (cylinder), Cone, and Box + 2 Ant (box shape with two antennas) are the most present shapes in LEO. Together, they represent 84.24% of the total amount of small objects in LEO. Table 1 summarizes the main shapes of small objects found in LEO with their mass ≤ 100 kg at the time of writing this paper.

Table 1. Main debris shapes found In LEO (mass ≤ 100 kg).

Shape	Amount	% of LEO Small Debris Total
Sphere	1044	25.08
Box	949	22.80
Box + 2 Pan	669	16.07
Cyl	457	10.98
Cone	274	6.58
Box + 2 Ant	113	2.72

On the other hand, Figure 2 shows the distribution of objects in LEO (mass ≤ 100 kg) grouped by their shape. Each dot represents a catalogued object relative to its apogee. The shape feature is ordered in descending order, where the sphere shape is the most present, and the Box + 2 Ant satellite shape is the least present.

The data analysis shows that, despite the wide variety of shapes, one generic shape is predominant in LEO: the Box shape (with or without solar panels or antennas). If our capturing mechanism targets all the different Box-shaped objects with mass ≤ 100 kg that exists in LEO (Box, Box + 2 Pan, Box + 2 Ant), it will have a clear impact on the debris problem at LEO. Indeed, the Box-shaped objects represent 41.59% of the total amount of small catalogued objects in LEO. Thus, actively catching Box-shaped debris helps answer the problem. Nano-satellites and mega-constellations are the future of LEO exploitation and will quickly saturate LEO. It is then essential to remove those satellites, even before

the 25 years of maximum stay in LEO proposed by Inter-Agency Space Debris Committee (IADC) guidelines [42].



Figure 2. Small objects' apogee and perigee distribution in LEO organised by main shapes.

The hybrid-compliant (the combination of passive and active) system proposed in this paper targets Box-shaped debris of various masses, not exceeding the 100 kg threshold. Other shapes can be considered in further work.

2.2. The Capturing Phase

An ADR mission consists of a succession of several crucial phases. From the launch of the spacecraft from Earth to the moment the chaser satellite, coupled with the debris, burns into the atmosphere, five general phases can be noted: berthed standby (the chaser satellite is on board and attached to the hosting platform), ejection (includes the launch of the rocket until the ejection of the payload), Far-Range Approach (arrive at hold point, close enough to the target), capturing, and post-capture (ready to de-orbit).

The capturing phase is the most crucial one. With little cooperation between the servicer and the target (no communication link, no fiducial markers, nor capture interfaces), capturing uncooperative debris is today one of the biggest challenges. Indeed, mission

failure and debris generation can occur more easily during that phase and the consequences can be dramatic.

Figure 3 describes the concept we propose for the capturing phase. It includes three sub-phases, pre-capture (approach guidance and control), soft-capture, and hard-capture; these are in charge of the approach preparation, the impact absorption and stabilization, and the securing of the debris attachment.

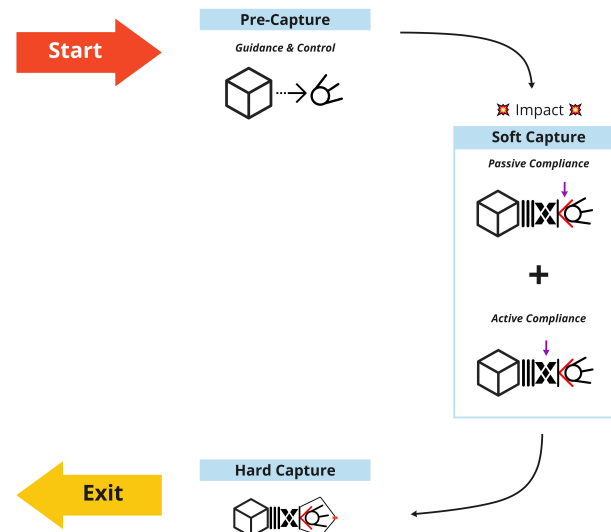


Figure 3. Concept of operations of our proposed capturing phase.

- **Pre-Capture**

The servicer satellite's guidance navigation and control (GNC) rendezvous and synchronizes its motion with the debris. The ADR system is, at first, undeployed inside the CubeSat architecture, as displayed in Figure 4, and is then deployed. At the end of the pre-capture approach, there is a relative distance d_t . Thus, only a translation motion is required to capture the debris.

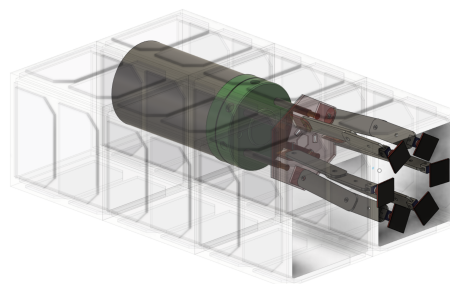


Figure 4. Undeployed hybrid-compliant system. The gray cylinder at the back of the system is for illustration purposes only.

- **Soft Capture**

In this sub-phase, the servicer satellite's thrusters are turned on to approach the debris and achieve the first contact. The first impact between the capturing mechanism and the debris must occur softly. Because of this, we propose a hybrid-compliant system for soft capture. It combines passive and active compliance with components that will reduce shocks and residual vibrations and actively control the contact time to avoid motion-reaction effects. It is assumed that the mechanism's tip will remain in contact with the debris for a finite time t_c , long enough to ensure that the hard capture mechanism secures the debris.

- **Hard Capture**

This sub-phase aims to secure the link between the servicer satellite and the debris, resulting in a reliable bond ready for deorbiting. After the soft capture, the hard capture mechanism will activate to fold and embrace the shape of the debris.

Figure 5 presents a general view of the proposed hybrid-compliant system for soft capture integrated into the CubeSat frame. This paper focused on the soft capture sub-phase. Details of the pre-capture and hard-capture sub-phases are out of the scope of this paper. Indeed, the system being at an early-stage design, we assume that the motion synchronization between the servicer and the debris had already been established in the pre-capture phase. Besides, the de-orbiting phase is considered out of the scope of the paper, as it is up to the servicer satellite using the proposed concept to decide how to demise the whole system with the debris attached.

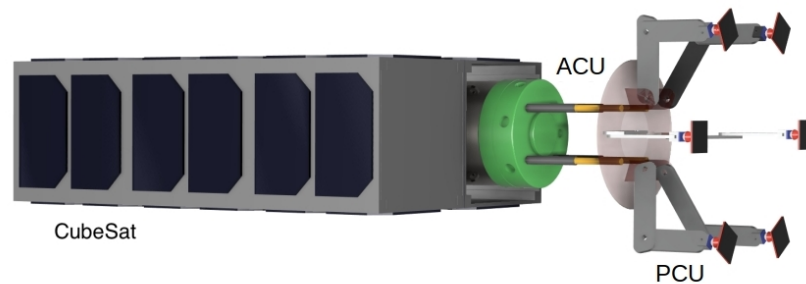


Figure 5. General view of a CubeSat-based hybrid-compliant system for soft capture of space debris. It includes the active compliance unit (ACU) and the passive compliance unit (PCU).

3. Hybrid-Compliant System for a Soft Capture of Space Debris

The high demand for reliability while capturing uncooperative debris makes the system be designed with compliance in mind first. A soft capture at the impact will ensure that the debris is not pushed away and give enough contact time for the capture. To guarantee this soft capture, this paper proposed a hybrid-compliant system at a conceptual level, with passive and active compliance, while fitting into a CubeSat architecture and considering the capturing of uncooperative box-shaped debris in LEO. Figure 6 presents a conceptual close-up view of the hybrid mechanism proposed for the soft capturing sub-phase. It comprises two crucial parts: the active compliance unit (ACU), with tunable stiffness, and the passive compliance unit (PCU), with a permanent stiffness. Together they form the soft capture Uunit (SCU) of adjustable stiffness of our capturing mechanism.

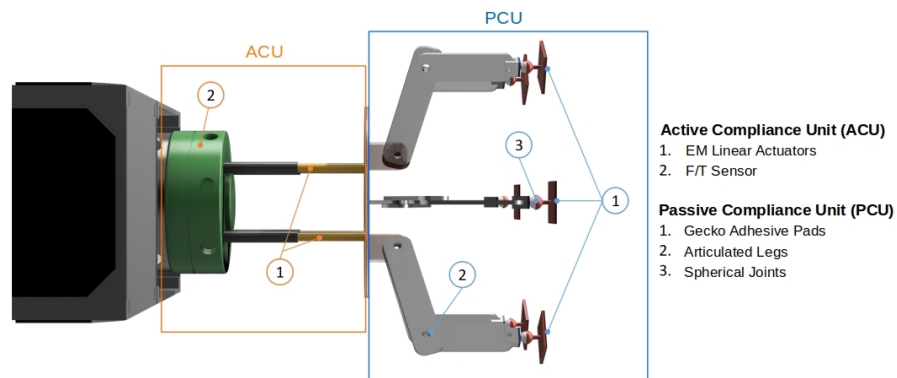


Figure 6. Closeup of the hybrid-compliant system for soft capture of space debris.

3.1. Passive Compliance Unit (PCU)

The PCU, as shown in Figure 6, has two main functions: to ensure a softer impact with the debris, as well as to adhere to the debris surface, both preventing it from moving away. This unit comprises three items: six articulated legs, six spherical joints, and six adhesive pads. The choice of having six legs lies in finding the right balance between the geometry of the system, its weight, and reliability, as fewer legs would question the system's redundancy. This part is the first of the whole system to encounter the target's surface.

- **Articulated Legs**

Each articulated leg, as shown in Figure 7, is composed of three aluminium parts linked together by revolute joints: the lower leg, the upper leg, and the link between the leg and the plate. The latter separates the PCU and the ACU. The passive compliance and flexibility feature is then made possible thanks to torsional springs located in the joints of the legs. The choice of adding torsional springs is for two reasons; to have a softer impact and better safety concerns regarding the system's integrity by avoiding high compression and bending constraints.

The torsional springs' stiffness will determine the PCU's maximum displacement in the axis of capture. This parameter plays an important role in the design of the overall hybrid compliance of the soft capture. Depending on the debris parameters (such as its mass), a too-low stiffness of the PCU could result in a longer displacement of the legs, and as a result, the system could break under the generated constraints. This point will be discussed later in Section 5.

- **Spherical Joints**

To link the legs to the adhesive pads, spherical joints are integrated. They give the pads two more mechanical degrees of freedom (in our case, two free rotations and the rotation in the axis of capture blocked), thus the better possibility to adapt to the debris surface. Indeed, in the case of a slight misalignment between the chaser satellite and the debris surface, the adhesion might not occur. In that regard, ensuring the parallelism of the pads with the debris surface is of utmost importance for efficient adhesion [43].

- **Gecko Adhesive Pads**

At the tip of each leg, a gecko-inspired dry adhesive [44] component is integrated as a thin layer under the pads. This dry, yet sticky, material must be activated by applying a shear force [43]. As a result, the microscopic "hairs" bend, creating a wider contact area between the pad and the target's surface, then making adhesion possible to many different material surfaces. These pads would also include a contact sensor [31] so that the control algorithms know exactly when to activate the adhesives. The shear force is created thanks to the active shrinkage of the legs towards the capture axis. This bio-inspired dry adhesive fits well for our case for two main reasons. Firstly, adhering within the required contact time to the debris surface is one way to avoid the action-reaction effect while creating sufficient time for securing the debris-chaser link. Moreover, selecting a dry adhesive that requires shear force to activate fulfils some of the requirements for this concept: besides being able to be used in a space environment [30], no additional normal force is required to adhere. Indeed, applying more contact force when one tries to avoid pushing the debris away sounds paradoxical. To that extent, getting a dry adhesive activated by shear force is the most suitable solution for catching space debris more reliably.

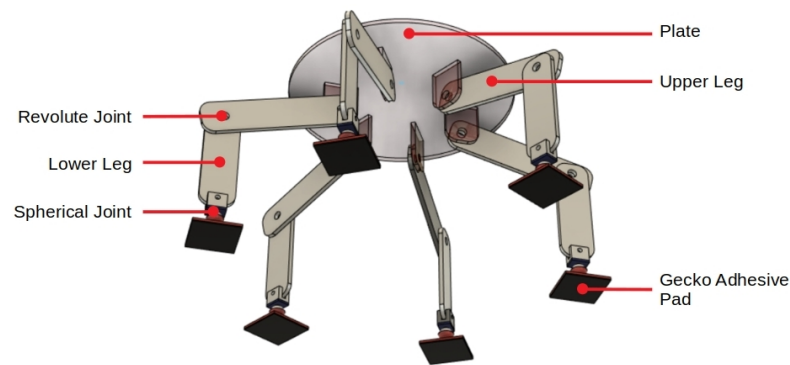


Figure 7. General view of the PCU, composed of one plate, six articulated legs, and six gecko-inspired dry adhesive pads.

3.2. Active Compliance Unit (ACU)

The ACU, as shown in details in Figure 8, is directly linked to the PCU with the same plate shown in Figure 7. This unit comprises four linear actuators linked with their base to a force/torque (F/T) sensor. Active compliance is ensured thanks to the active control of the linear actuators along the capture axis. Details about the controller are presented in Section 4. By actively changing the stiffness of the ACU, it is possible to ensure a sufficient contact time to actuate the other parts of the ADR capturing process. This allows the system to target a wider range of debris without fundamentally changing its conceptual design.

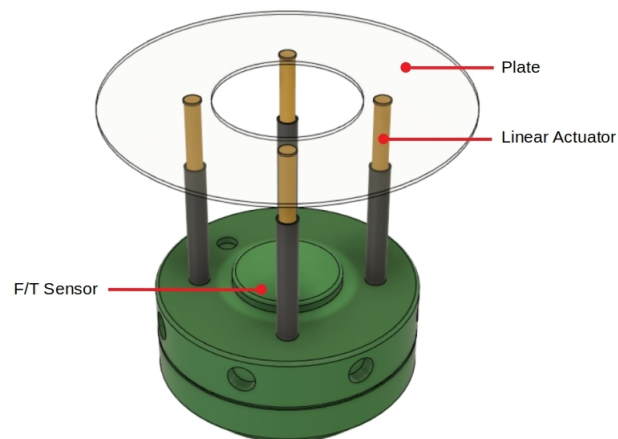


Figure 8. General view of the ACU. The CDU is composed of one force/torque sensor, four electromechanical linear actuators and one plate.

- **Force/Torque Sensor**

The presence of an F/T sensor, as seen in green in Figure 8, helps feed the controller with the force encountered at the impact between the chaser satellite and the debris. Consequently, the linear actuators will be actuated regarding the force sensed by the F/T sensor, providing the required equivalent stiffness of the overall system towards the targeted debris. This means one can change the parameters of the stiffness and damping of the ACU.

- **Electromechanical Linear Actuators**

The four linear actuators are an essential part of the ACU. They are represented in Figure 8 with the static part in gray and the dynamic part in yellow. Although a single linear actuator would have performed the task properly, a failure in that system can generate mission failure. In that regard, it is important to ensure better reliability of that part of the system by using four redundant electromechanical linear actuators. The linear motion of

the actuators makes them act as a spring and damper system in a controlled way. As a result, active compliance is created with the F/T sensor in a control loop.

3.3. Soft Capture Process

Both the ACU and the PCU will work together towards a successful soft capture of the space debris, as described in Section 2.2. As a reminder, the main goal of the soft capture sub-phase is to absorb the impact and welcome, as softly as possible, the debris while retaining it from moving away. During the capture process, the actions of the soft capture can be depicted in four main steps, as displayed in Figure 9: the Initialization, the first contact, the hybrid compliance operation (active and passive compliance occurs simultaneously), and the adhesive activation. Video S1 attached to this paper provides a visual understanding of the described steps.

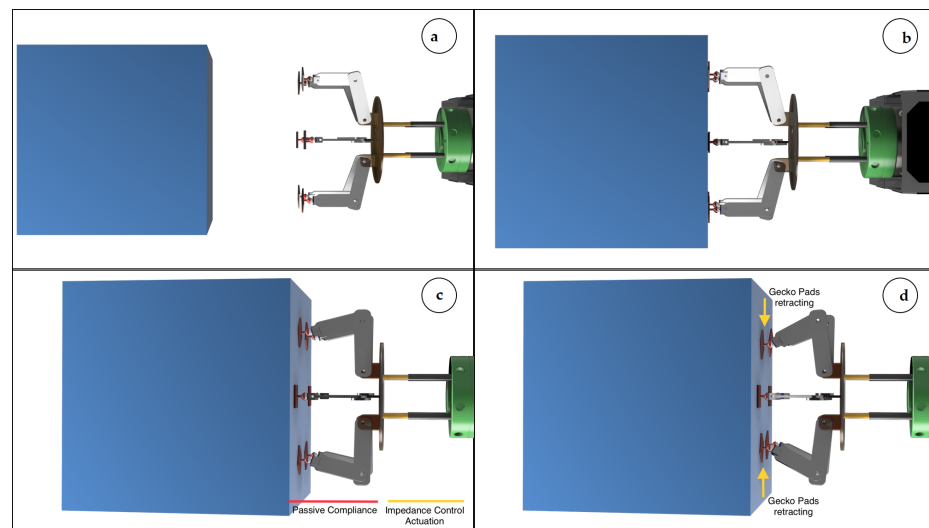


Figure 9. Soft capture process of the proposed ADR concept: (a) initialisation; (b) first contact; (c) hybrid compliance operation; (d) adhesive activation.

- **Initialisation**

At this moment of the process, the ADR system is already deployed, and only a relative distance d_t separates the servicer satellite from the debris. The servicer satellite approaches the debris with a translation motion, as depicted in the first image in Figure 9a.

- **First contact**

The PCU is the part which arrives in contact with the flat surface of the debris first, with its gecko adhesive pads parallel to the debris surface, as shown in Figure 9b.

- **Hybrid Compliance Operation**

As the contact is made, the flexible legs articulate instantly, as seen in Figure 9c, providing the first damping of the impact's vibrations and not being too close to an elastic collision between the two entities (where both momentum and kinetic energy are conserved). The fixed stiffness of the PCU lets the legs articulate while keeping in contact with the debris surface.

At this time of the process, the PCU is not the only one acting; the ACU is also activated at the impact. As soon as there is contact between the SCU and the debris, the force exerted in the axis of capture on the ADR system's tip is fed into the controller of the ACU. As a result, the electromechanical linear actuators are put into action accordingly, reducing their length (as shown in Figure 9c) and thus providing an additional set of virtual springs and dampers based on the contact's force. The contact time t_c between the tip of the capturing system and the debris can then be controlled thanks to the ACU.

- **Adhesive Activation**

The action of passive and active compliance is performed within that time frame of t_c seconds, giving the required theoretical time for the adhesive activation to occur, which is essential to the mission's success. The last goal of the soft capture sub-phase (retaining the debris from moving away due to the action-reaction effect) is made possible by creating adhesion on the debris surface. Within the contact time t_c , the adhesive pad's contact sensors must send a positive signal to the ADR system's process controller and activate the pads' shrinkage, as shown in Figure 9d. Working in opposite pairs, the pads are pulled towards the longitudinal axis of the capture, towards the centre of the ADR tip's plane; shear force is necessary to adhere. That shear force is maintained to keep the adhesives activated, retaining the debris from moving away.

Once the bond is created between the servicer and the debris, the soft capture sub-phase is performed, and the capture phase can proceed.

4. Impedance Controller

To actively remove space debris, a servicer CubeSat will have to perform the final approach, deploy the dedicated mechanism, and then perform the capturing phase of the ADR mission. Having a hybrid-compliant system implies that both *passive* and *active* compliance are involved. Since the passive compliance has fixed stiffness and damping coefficients, it is required to analyse and model the adequate controller to get the active compliance's right coefficients. The CubeSat and the debris are specific in mass, but the capturing mechanism's compliance can be modified for the optimal response of the ADR system regarding the contact time with the debris. In this section, the aim was to study the behaviour of the systems during contact and then regulate the relationship between the ADR system's tip and contact force, employing an impedance controller. A single-axis analysis was undertaken (central impact), as is common in the literature [45].

4.1. System Modeling

The servicer satellite, consisting of a main body (CubeSat), and the hybrid compliant system for soft capture, is modelled as a three-body equivalent system, as represented in Figure 10. The CubeSat, along with the ACU's F/T sensor and the fixed part of the ACU's linear actuators, are lumped into the first rigid body with mass m_s . The moving part of the ACU's actuators, the plate that separates ACU and PCU, and the PCU's upper legs are lumped into a second rigid body with mass m_e ; while the lower legs and the gecko adhesive pads are lumped to a third rigid body having mass m_c . The positions of the center of mass (CoM) of m_s and m_e are denoted by x_s and x_e , and the position of the mechanism's tip is denoted by x_c . The debris is modelled as a rigid body of mass m_d , and the position of the point on the debris that comes into contact with the mechanism's tip is denoted by x_d .

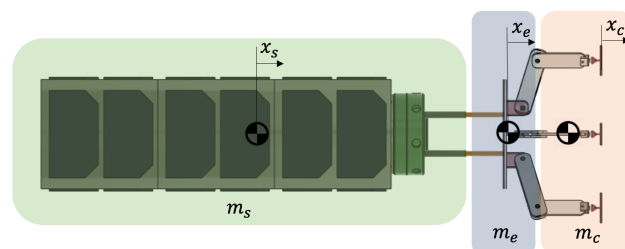


Figure 10. Equivalent three-body system of the CubeSat and ADR system.

Masses m_s and m_e are connected through linear actuators, allowing a translation degree of freedom to be controlled. The maximum displacement of the linear actuators' moving parts is denoted by l_a . Masses m_e and m_c are connected through passive compliance, with stiffness k_s and damping b_s , that models the compliance provided by the 6 torsional springs located in the revolute joints of PCU's legs shown in Figure 7. Figure 11 provides a simplified 2D view of the three-body system.

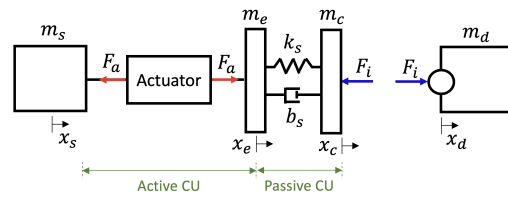


Figure 11. Schematic of the equivalent three-body CubeSat-ADR system.

Before the contact, the CubeSat-ADR system has a non-zero relative velocity with respect to the debris. Once the PCU’s mass m_c arrives in contact with the flat surface of the debris mass m_d at the moment t_i , m_c and m_d have the same position, i.e., $x_c = x_d$, the passive compliance enters into motion instantly, and the impedance controller is activated.

The aim of the simulation study was to showcase the importance of incorporating active and passive compliant components to dissipate impact energy, ensure contact time, and enhance the capture of a wider range of space debris masses. Therefore, the simulation study was based on the following assumptions. The motion synchronization between the servicer and the debris was established, resulting in a zero relative angular velocity. The desired contact point of the ADR system’s tip on the debris was assumed to pass through the debris centre of mass, resulting in only a contact force and no external moment on the debris. The assumption was made that the centre of mass of the debris is known, supported by existing research on estimation techniques. Misalignments during realistic approach and contact were not considered and flat surfaces were assumed for both the ADR system and debris, generating contact force along the approach and contact axis.

Based on these assumptions, a three-dimensional simulation of the equivalent three-body system yields single-axis motion for the servicer and the ADR system was performed, providing informative data along the approach and contact axis. Due to the absence of relative rotational motion, all motion occurs along this axis. The inclusion of the assumption of point masses in the simulation model, neglecting the moment of inertia, does not affect the study’s conclusions. The paper presents the equations of motion for this equivalent system, focusing on the commonly employed central impact analysis of the single motion axis.

Specifically, the system equations of motion for each of the three rigid bodies of the equivalent CubeSat-ADR system in Figure 11 with masses m_s , m_e , and m_c , and for the space debris with mass m_d , obtained during the contact between m_c and m_d , are given by Equations (1), (2), (3) and (4), respectively.

$$m_s \ddot{x}_s = -F_a \tag{1}$$

$$m_e \ddot{x}_e = F_a + k_s(x_c - x_e - l_s) + b_s(v_c - v_e) \tag{2}$$

$$m_c \ddot{x}_c = -F_i - k_s(x_c - x_e - l_s) - b_s(v_c - v_e) \tag{3}$$

$$m_d \ddot{x}_d = F_i, \tag{4}$$

where F_a is the commanded force applied on the capture unit by the impedance-controlled linear actuator, l_s is the physical length of spring k_s , and F_i is the impact force between the mechanism’s tip and the debris. All forces are shown in Figure 11.

4.2. Design of the Impedance Controller

For successful adhesion, the required contact time between the ADR system’s tip and the debris must be ensured; thus, its adjustment is required. This adjustment was achieved by altering the ADR system’s impedance. Therefore, an impedance controller with tunable gains was developed. Specifically, impedance control attempts to implement a dynamic relation between the ADR system’s variables, such as tip position and contact force, rather than just controlling these variables alone [37].

Subsequently, the controller needs to be informed, which is the wanted relation between the ADR system’s variables during impact i.e., the desired system’s behavior. The equation selected to describe this behavior is called *impedance filter* and is shown in Equation (5), [34,46]. It consists of three terms: one for the desired inertia m_f to be seen at the tip, one for the desired damping b_f , i.e., the desired relationship between contact force and tip’s velocity, and one for the desired stiffness k_f , i.e., the desired relationship between contact force and tip’s displacement [37].

$$m_f(\ddot{x}_c - \ddot{x}_s) + b_f(v_c - v_s) + k_f(x_c - x_s - l_m) = -F_i. \tag{5}$$

The desired contact time of the ADR system with the debris and, thus, the success of capturing directly, can be realized by tuning the mass, spring, and damper impedance parameters m_f , b_f , and k_f , respectively. Parameter l_m in Equation (5) is the initial distance between m_c and m_s .

Substituting \ddot{x}_s of Equation (1) and \ddot{x}_c of Equation (3) into the impedance filter in Equation (5), and then, solving for the applied actuator force by the impedance controller F_a required to achieve the desired impedance behavior of Equation (5), yields

$$F_a = \frac{m_s}{m_f} \left(\frac{m_f}{m_c} - 1 \right) F_i + \frac{m_s}{m_f} k_f (x_s - x_c + l_m) + \frac{m_s}{m_f} b_f (v_s - v_c) + \frac{m_s}{m_c} k_s (x_c - x_e - l_s) + \frac{m_s}{m_f} b_s (v_c - v_e). \tag{6}$$

The impedance parameter m_f is selected equal to m_c so that the actuator force F_a does not depend on the impact force F_i [34]. Then, the applied actuator force F_a is given by

$$F_a = k_p (x_s - x_c + l_m) + k_d (v_s - v_c) + \frac{m_s}{m_c} k_s (x_c - x_e - l_s) + \frac{m_s}{m_c} b_s (v_c - v_e), \tag{7}$$

where the controller’s gains k_d and k_p are given by

$$k_p = \frac{m_s}{m_c} k_f \tag{8}$$

$$k_d = \frac{m_s}{m_c} b_f. \tag{9}$$

To calculate the gains based on Equations (8) and (9), the impedance parameter k_f must be selected. Furthermore, choosing critical damping results in the impedance parameter b_f .

$$b_f = 2\sqrt{m_f k_f}. \tag{10}$$

The impedance control loop is shown as a block diagram in Figure 12.

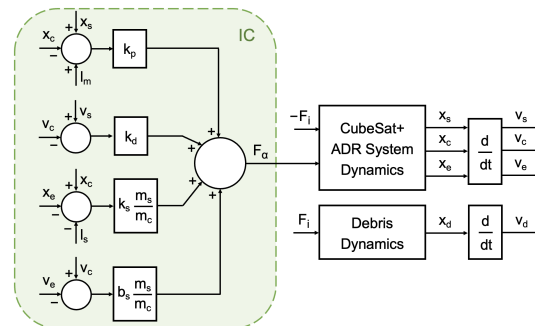


Figure 12. Block diagram of the impedance control strategy for the soft capture of space debris.

4.3. Hybrid Compliance

The useful terms of *active* and *hybrid* compliance are described in this section to understand the proposed impedance controller better. For this purpose, we used a reduced version of the three-mass system previously described in Figure 11. The reduced version is

a two-mass equivalent ADR system with only the ACU to control its interaction with the debris, as presented in Figure 13a.

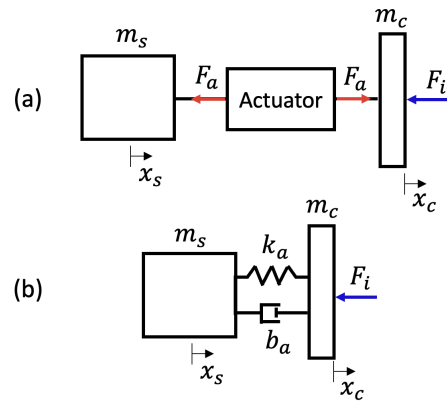


Figure 13. CubeSat-ADR system with two masses connected by (a) impedance-controlled actuators, (b) an active (virtual) compliance equivalent to (a).

The system equations of motion for the equivalent ADR system in Figure 13a, during the contact with the debris, can be written as:

$$m_s \ddot{x}_s = -F_a \tag{11}$$

$$m_c \ddot{x}_c = -F_i + F_a. \tag{12}$$

Substituting \ddot{x}_s of Equation (11), and \ddot{x}_c of Equation (12), into the impedance filter that describes the desired impact behavior of Equation (5) yields

$$-\frac{m_f}{m_c} F_i + \frac{m_f}{\mu_{ef}} F_a + b_f (\dot{x}_c - \dot{x}_s) + k_f (x_c - x_s - k_m) = -F_i, \tag{13}$$

where μ_{ef} is given by

$$\mu_{ef} = \frac{m_c m_s}{m_c + m_s}. \tag{14}$$

Solving for the actuator force F_a and selecting m_f equal to m_c so that F_a does not depend on the impact force F_i , yields

$$F_a = k_p (x_s - x_c + l_m) + k_d (\dot{x}_s - \dot{x}_c), \tag{15}$$

where k_d and k_p are the impedance controller’s gains given by

$$k_d = \frac{\mu_{ef}}{m_f} b_f \tag{16}$$

and

$$k_p = \frac{\mu_{ef}}{m_f} k_f. \tag{17}$$

Observing Equation (15) for the actuator’s force command F_a , one can conclude that the impedance-controlled actuator behaves in active (virtual) compliance with spring coefficient k_a of length l_a and damping coefficient b_a , as shown in Figure 13b; in this example, equal to the controller’s gains k_p and k_d , respectively.

Furthermore, the proposed ADR system, as modelled in Section 4.1 and shown in Figure 11, incorporates, additionally to the active compliance, passive physical compliance with spring coefficient k_s of length l_s and damping coefficient b_s , see Figure 14a.

The active and the passive compliance in series can be combined to form an equivalent hybrid compliance of length $l_m = l_s + l_a$ with spring coefficient k_m and damping coefficient b_m as shown in Figure 14b.

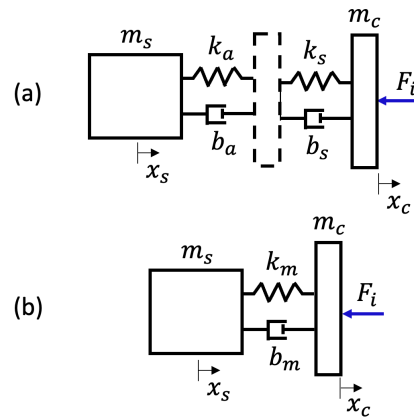


Figure 14. CubeSat-ADR system as two masses connected by (a) a passive and active compliance in series, (b) a hybrid compliance, equivalent to (a).

The stiffness and the damping coefficients k_m and b_m of the hybrid system are of paramount importance as they affect the ADR system’s impedance, the contact time of the ADR system with the debris and, thus, the success of the debris capture. Therefore, the reduced hybrid-compliant system shown in Figure 14b is used in Section 5.4 to showcase the necessity of hybrid compliance in an ADR system.

5. Simulation Study and Results

A series of simulations were conducted with three objectives in mind: to study the relationship between the debris mass and the required compliance and to demonstrate the importance of the proposed hybrid compliant system (Section 5.2); to study the impact of the design parameter l_m (Section 5.3); and to test the impedance controller and analyze its role to achieve a soft capture of space debris (Section 5.4).

5.1. Simulation Setup

The simulations were run in MATLAB/Simscape using a variable-step ode45 solver. The Simscape model, consisting of the hybrid-compliant system mounted on the servicer CubeSat and the space debris, were developed for the simulations. During the simulations, the positions and velocities of the masses under the impact and their interpenetration were calculated. This was fed back to a contact model and a force was generated, pushing away the masses under impact. The contact time t_c was calculated based on the impact force.

The developed contact model uses the visco-elastic theory. According to this theory, a compliant surface under impact can be modelled by a combination of lumped parameter elements, i.e., springs and dampers. This study calculated the contact force between the bodies under impact using the Kelvin–Voight model [47]. Assuming that the impact is close to an elastic (no damping), the impact force is given by:

$$F_i = k_i(x_c - x_d), \tag{18}$$

where x_c is the position of the mechanism’s tip and x_d is the point on the debris that comes into contact with the mechanism’s tip. In this study, stiffness k_i was equal to 10,000 N/m [48,49] and, thus, the contact was assimilated to a very stiff spring, activated when x_c is greater than x_d .

The CubeSat-ADR system has a small relative velocity set to 10 mm/s with respect to the debris. The CoM’s initial position x_s , of mass m_s , equals zero before impact. The initial position of x_c equals l_m (l_m is defined in each experiment). The debris’ initial position relative to the ADR system’s tip, denoted by $x_d - x_c$, was set equal to 10 cm without

loss of generality since, in the simulation, the ADR system approaches the debris with a constant velocity v_s . Equivalent systems' point masses m_s , m_c , and m_e (when applicable) are 12.0012 kg, 0.024 kg, and 0.016 kg, respectively.

5.2. Debris-Mass and Compliance Relation

As the masses of the servicer CubeSat, including the ADR system, were assumed to be known, the desired stiffness and the damping coefficients of the hybrid system's equivalent compliance must be selected. The selected parameters should ensure that the minimum contact time between the ADR system and the debris was achieved. An analytical solution for the optimal tuning of these coefficients is difficult to obtain since no analytical equation relates the contact time and the hybrid compliance coefficients. Because of this, an algorithm in MATLAB, consisting of a loop, was developed to search the successful cases ($t_c >$ minimum contact time required) in a range of stiffness values, for a range of space debris masses and for a range of minimum contact time required to complete the capture.

Specifically, the servicer CubeSat and the ADR system were simulated when approaching and coming into contact and the success in terms of the time of contact was noted. It was considered a successful case if it was greater than the contact time required for the successful capturing while not reaching the spring limit. Then, the corresponding spring's stiffness and the debris mass were stored.

In this simulation study, for tuning the hybrid compliance of the system, the servicer CubeSat and the ADR system were modelled as a two-mass equivalent system, i.e., as two point masses connected by the hybrid compliance, as shown in Figure 14b. This compliance was considered hybrid since it consists of passive parts integrated into the PCU and the active part realized by the impedance-controlled linear actuator of the ACU, as shown in Figure 14a.

The stiffness and damping coefficients to be altered during the search of the developed algorithm are denoted by k_m and b_m , respectively. Once k_m is altered, by choosing critical damping, one can calculate b_m too, as follows

$$b_m = 2\sqrt{m_c k_m}. \tag{19}$$

The hybrid compliance's length l_m is equal to 0.05m since it is the sum of two lengths: $l_m = l_s + l_a$; the length l_s of the passive physical compliance, equal to 0.025 m, and the maximum displacement l_a of the linear actuators' moving parts, equal to 0.025 m. The schematic of the system under simulation study as designed in Simscape is shown in Figure 15.

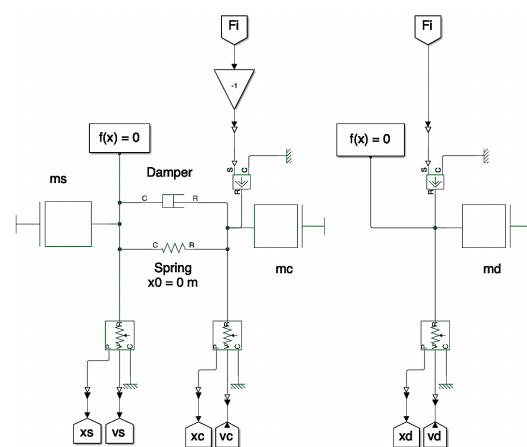


Figure 15. Schematic of CubeSat-ADR system and debris in Simscape.

The algorithm runs for the range of stiffness values k_m between [0.1–0.5] N/m, with a step of 0.1 N/m, for a range of space debris mass m_d between [1–100] kg, with a step of 1 kg, and for a range of minimum contact time t_c required for completion of the capturing between [4–12] s, with steps of 2 s.

The resulting diagram is shown in Figure 16, providing the relation between these variables. More detailed visualization of the data of Figure 16 is provided for each contact time in the range of [4–12] s in Appendix A. The lines depicted in the 3D diagram correspond to points in 3D space, representing the successful cases obtained from the algorithm. Each point along the line represents three distinct values, namely: space debris mass, minimum contact time achieved, and hybrid compliance stiffness coefficient.

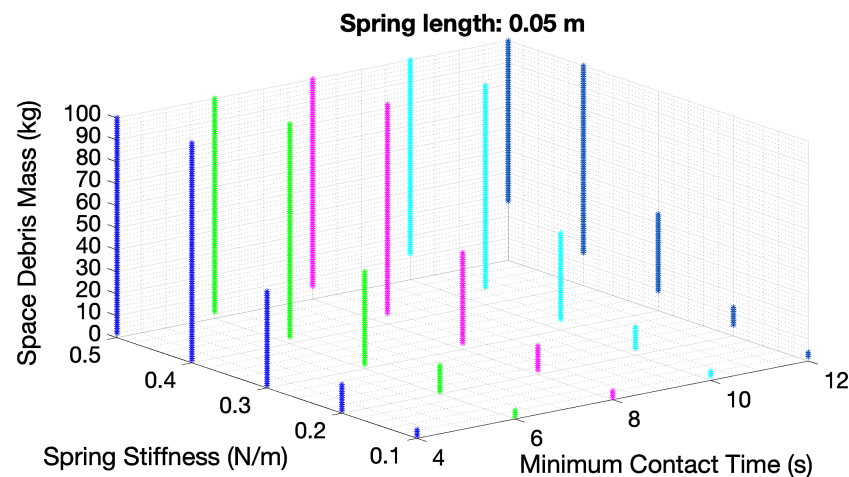


Figure 16. Range of space debris masses to be targeted for different stiffness coefficients and minimum contact times achieved.

Note that the [4–12] s range for this simulation for the minimum contact time required was selected since it was sufficient to showcase the necessity of tuning the system’s compliance and, therefore, of the hybrid compliance concept. Simulation results for minimum contact time required greater than 12 s show that hybrid compliance is even more necessary if we want to target a wide range of debris between 0–100 kg. This can be easily shown by the trend shown in Figure 16: the minimum contact time required increases, and the range of debris masses to be targeted decreases. Moreover, a contact time of less than 4 s for successful capturing is considered unrealistically small.

Based on the diagrams, desired stiffness and damping coefficients of the hybrid system’s equivalent compliance can be selected for a specific debris mass and minimum contact time required.

In Figure 16, the relation of the variables is derived. In particular, when the equivalent stiffness increases for a specific minimum contact time, the range of the debris masses increases and the minimum debris mass to be targeted increases. One could say that small stiffnesses are appropriate for targeting a small range of small debris and larger stiffnesses are appropriate for targeting a wider range of debris masses of larger debris masses. Furthermore, when the minimum contact time required increases, the maximum debris mass to be targeted remains constant for a specific spring stiffness due to displacement limitations of the compliant parts and the minimum debris mass that can be targeted increases. Thus, when the minimum contact time required increases, the range of debris masses to be targeted decreases.

5.2.1. Indicative Case

In this section, indicative plots are presented based on the simulation responses for a specific set of values in the range searched by the algorithm. Specifically, the indicative plots in this section were obtained using a simulation with k_m and b_m equal to 0.5 N/m and 0.1789 Ns/m, respectively, and debris with mass m_d equal to 12 kg. The positions of the point masses m_s , m_c and m_d are shown in Figure 17. As shown in this figure, the tip of the ADR system was initially located 10 cm from the debris. For almost 10 s, the ADR system approaches the debris, moving together while in contact.

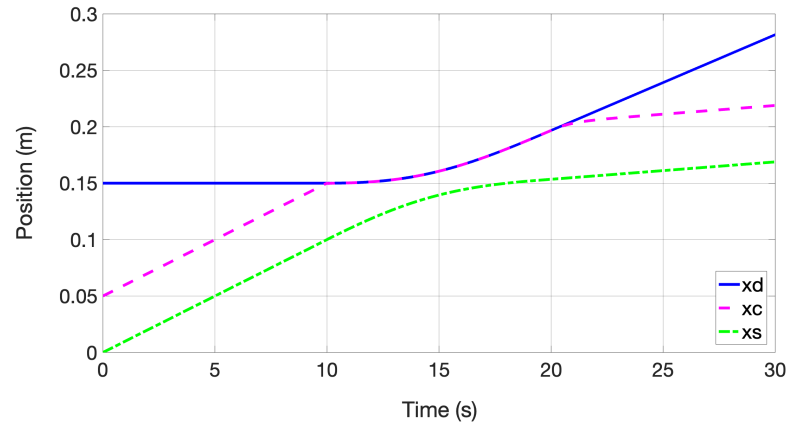


Figure 17. Position of masses for the indicative case.

The contact time t_i was calculated using the impact force shown in Figure 18. It is the time when the impact force is continuously greater than zero and, thus, is equal to 10.12 s. The impact force in Figure 18 was set to zero when the relative position of the ADR system’s tip from the debris, shown in Figure 19, was negative, indicating that there is a distance between the two systems. However, when the systems are in contact, the interpenetration of the bodies, shown in Figure 19, is positive, and the impact force was calculated based on Equation (18); it is the multiplication of the spring stiffness k_i times the interpenetration in Figure 19.

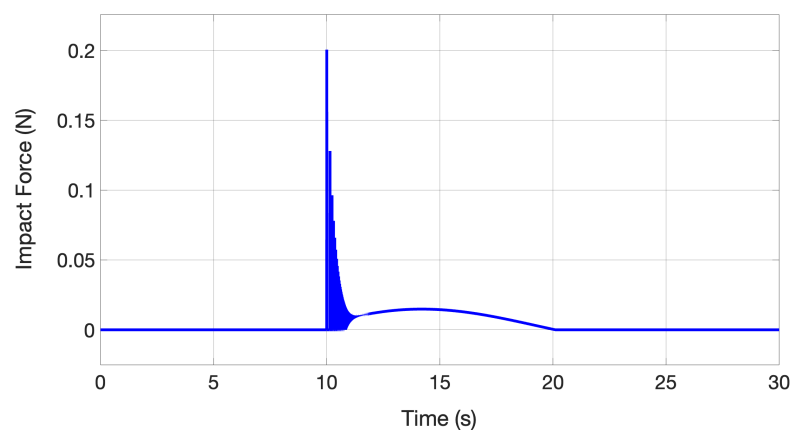


Figure 18. Impact force for the indicative case.

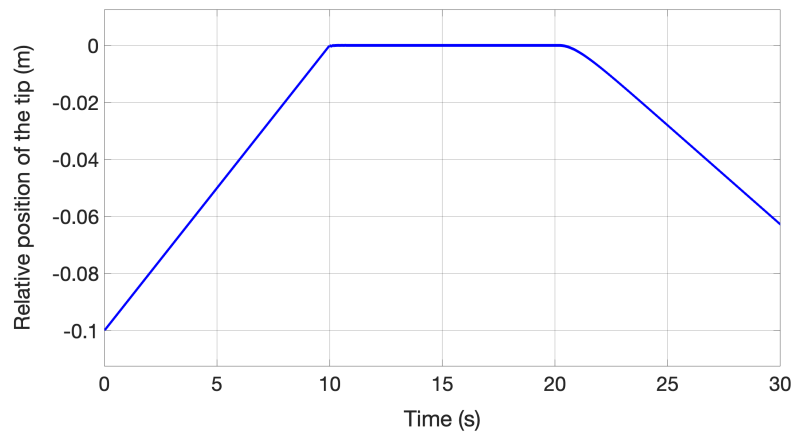


Figure 19. Relative position of ADR system’s tip with regard to the debris contact point for the indicative case.

5.2.2. Discussion: The Need for Hybrid Compliance

The analysis of the diagram in Figure 16 leads to a conclusion of major importance regarding the design of the ADR system itself. When the required minimum contact time is very small, there is indeed an appropriate stiffness coefficient for targeting most debris masses in the desired range of 0–100 kg. However, for more realistic minimum contact times required, none of the stiffness coefficients are adequate; one must be able to modify the equivalent spring’s stiffness to target the whole desired range of debris.

Considering the use case where the system only uses the benefits of passive compliance, the equivalent stiffness would remain constant without any possibility of being tuned. In that regard, the range of debris that can be targeted is consequently constrained. Assuming a passive spring of 0.5 N/m, and the required minimum contact time is 10 s, based on the diagram in Figure 16 and the more detailed visualization of it provided in Figure 20, the range of debris masses that can be targeted is 12–100 kg. Nevertheless, to capture debris of smaller mass, e.g., 4 kg, an equivalent stiffness coefficient of 0.2 N/m would be required for the equivalent spring, as shown in Figure 20. To achieve the tuning of the spring’s stiffness from 0.5 N/m to an equivalent spring’s stiffness of 0.2 N/m, active compliance should be added, realized by an impedance controller, adding versatility to the system.

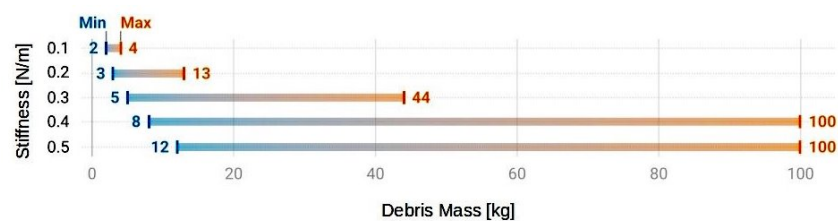


Figure 20. Detailed visualization of Figure 16 for minimum contact time achieved of 10 s. Range of debris masses for different stiffness coefficients.

To decrease the equivalent spring stiffness k_m to make it equal to 0.2 N/m, the additional active compliance k_a should be in series with the already-manufactured and integrated passive one k_s , with k_s equal to 0.5 N/m in this study. Hence, based on Equation (20) for springs in series, the stiffness coefficient of the active compliance k_a should be equal to 0.333 N/m. Employing this active compliance in the presence of the passive one, the debris of 4 kg can be successfully captured, thus allowing the ADR system to target a wider range of debris than the one targeted by employing only the passive compliance.

$$k_m = \frac{k_s k_a}{k_s + k_a} \tag{20}$$

One could wonder why not use only active compliance. For reliability reasons, integrating flexibility with passive compliance at the first impact interface would avoid a hard shock and, thus, avoid pushing away the debris. Moreover, if the debris has an unexpected mass variation, tuning the stiffness brings more reliability and safety, reducing the risk of damaging either the servicer or the debris itself.

5.3. Impact of the Compliance's Physical Length

The series of simulations and results are presented in Figure 16 and in Appendix A, considering a length l_m of the equivalent spring equal to 0.05 m. The physical length of the spring denotes the available space of the mechanism to compress, as shown for the indicative case in Figure 21. It is, therefore, an important design parameter for the system.

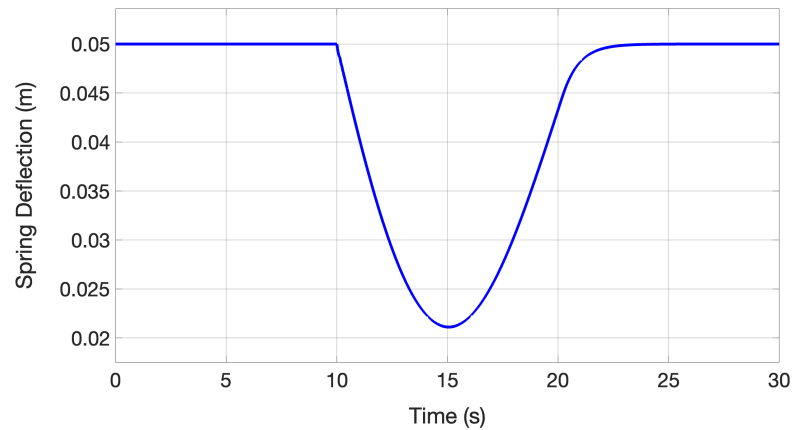


Figure 21. Spring deflection for the indicative case.

A series of simulations were run for a different spring's length to further enhance the discussion and the valuable conclusions. The algorithm developed searches for the range of stiffness k_m between 0.25–1.25 N/m, for a range of space debris mass m_d between 1–100 kg and for a range of minimum contact time required for completion of the capturing between 5–8 s. Specifically, Figure 22 displays the range of space debris masses that can be targeted and successfully captured for a range of equivalent spring stiffnesses and for various minimum contact times required for a spring's length l_m equal to 0.025 m.

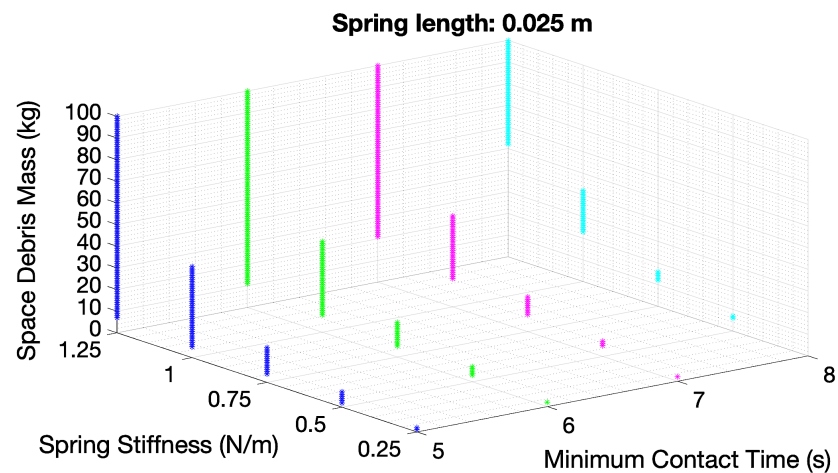


Figure 22. Range of space debris to be targeted for different contact times.

Based on this diagram, one could observe that, for a specific minimum contact time and spring’s stiffness, the range of debris masses that can be targeted is smaller than the corresponding one when the spring’s length l_m is equal to 0.05 m. This is because, at similar stiffnesses and contact time parameters, the retracting phase on the spring reaches its limit, resulting in possible damage to the servicer CubeSat. In other words, the contact time requirement may be fulfilled while reaching the spring’s length limits, which may be dangerous for the servicer satellite. Hence, the ability to tune the equivalent stiffness coefficient using an impedance controller is even more necessary. Moreover, as shown in Figure 22, the maximum contact time achieved is no more than 8 s; this is an important contact time constraint. In conclusion, for an ADR system to target a wider range of debris masses while ensuring a realistic required time of contact, the spring’s length for compliance—or alternatively the space that the system has to compress—must be carefully selected to be above a minimum value.

5.4. Evaluation of Hybrid Compliance

Two versions of the ADR system were simulated to further demonstrate the importance of tuning the ADR system’s compliance by adding an active compliant unit and to showcase the application of the proposed impedance controller. Subsequently, the responses were measured and the corresponding contact times were calculated and compared.

The first system is a passive system, denoted as PCS, composed only of passive physical compliance. In this case, the ACU is inactive; thus, its prismatic joints are locked, see Figure 23a. The second system is a hybrid-compliant system, denoted as HCS and shown in Figure 23b, composed of passive and active compliance; the linear actuators apply forces F_a driven by the proposed impedance controller presented in Section 5.2 and given by Equation (7).

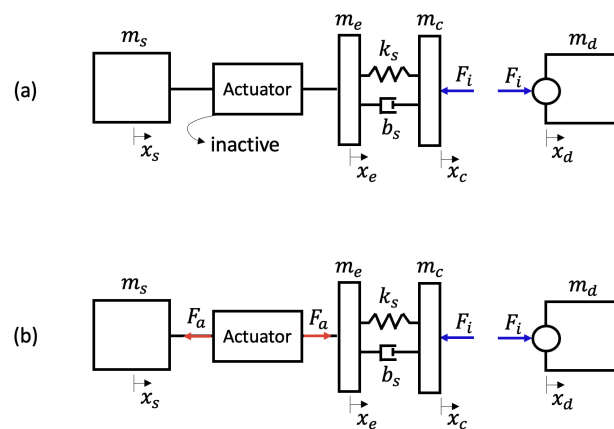


Figure 23. Comparison of ADR systems; (a) PCS: system with only passive compliance (inactive linear actuators); (b) HCS: hybrid system with both passive and active compliance.

The passive compliance’s stiffness k_s equals 0.5 N/m following the use case presented in Section 5.2 and its physical length l_s is equal to 0.025 m. The linear actuator’s space limit, i.e., the maximum displacement $l_a = x_e - x_s$ allowed, is also equal to 0.025 m.

Figure 24 shows the impact force generated at the tips of the PCS system (magenta line) and the HCS system (blue line). Figure 25 shows the actuator force commanded by the impedance controller to be less than 0.15 N.

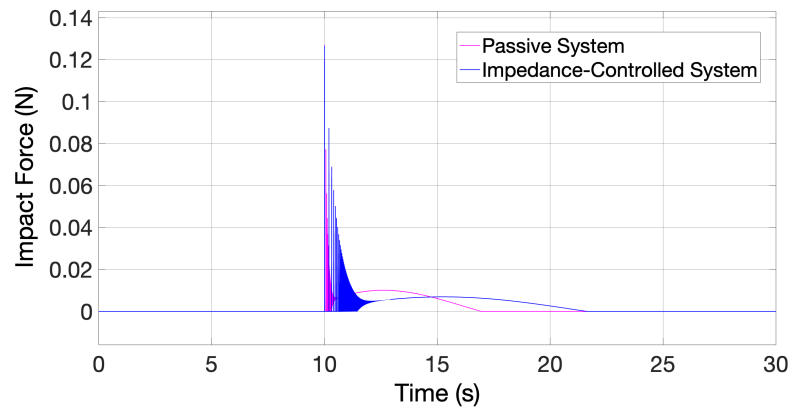


Figure 24. Comparison of impact forces of passive and impedance controlled systems.

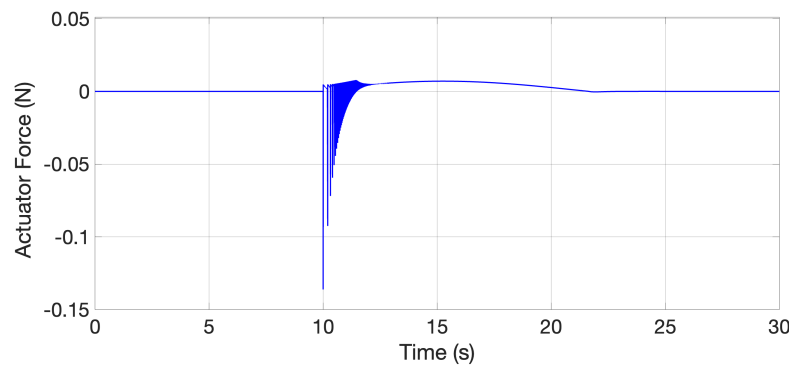


Figure 25. Commanded force by the impedance-controlled linear actuator.

Observing Figure 24 and comparing the contact times, one can see that using the proposed impedance controller significantly increases the contact time from 7 s to 11.65 s. Hence, the applied controller adjusted the contact time between the ADR system’s tip and the debris and ensured the minimum required; in this example, equal to 10 s. The desired contact time of the ADR system was ensured by the appropriate tuning of the mass, spring, and damper impedance parameters m_f , k_f , and b_f of Equation (5), respectively, and therefore of the IC gains.

To find the appropriate impedance parameters m_f , k_f , and b_f , the simulation results provided in Section 5.2 for the use case were employed. Specifically, to capture debris with a mass of 4 kg, the required hybrid compliance’s stiffness and damping coefficients, k_m and b_m , were found to be equal to 0.2 N/m and 0.17 Ns/m, respectively. Thus, the desired spring and damper parameters of the impedance filter k_f and b_f can be calculated based on Equation (16) as

$$k_f = \frac{m_f}{\mu_{ef}} k_m \tag{21}$$

and,

$$b_f = \frac{m_f}{\mu_{ef}} b_m, \tag{22}$$

to be equal to 0.2003 N/m and 0.1702 Ns/m, respectively. The desired mass parameter m_f is equal to m_c . Using the desired impedance parameters m_f , b_f , and k_f derived, the IC gains k_p and k_d were calculated based on Equations (8) and (9) to equal 150 N/m and 128 Ns/m, respectively. The IC command F_a , which drove the ACU’s linear actuators, was calculated by Equation (7).

The application of the IC implemented active (virtual) compliance into the ADR system, rendering it a hybrid-compliant system. Comparing the PCS and HCS, the necessity of the IC and, subsequently, of a hybrid-compliant ADR system for the successful capturing of debris, was validated.

6. Conclusions

This paper proposed a one-to-many solution: a flexible, versatile capturing mechanism of class ET2 targeting a vast range of small uncooperative space debris in low Earth orbit (LEO). It incorporates a hybrid-compliant system, combining active compliance (with controlled linear actuators) and passive compliance (with legs articulated by torsional springs). Combined, they make the equivalent hybrid stiffness adjustable to a specific range of debris mass. This novel system also uses a bio-inspired dry adhesive to stick to the debris surface and keep it from being pushed away, increasing the overall reliability of the ADR mission.

The simulation study presented in this paper revealed that a passive-compliant ADR system was incapable of targeting all the small debris. The integration of both active and passive compliance was required to enable the successful soft capturing of the whole range of small debris (up to 100 kg). It allows the system to gently welcome the debris in contact with the servicer satellite, providing the required contact time for properly capturing it. The active compliance is controlled by the developed impedance controller (IC), which adjusts the compliance parameters based on the debris that will be captured.

This paper brings forward the research on capturing a wide range of small debris in orbit, thus contributing to a cleaner and safer space. Future work will focus on the design, development, assembly, verification, and validation (V&V) of all components of the mechanism and experimental V&V testing in the Zero-G Lab facility of SnT-University of Luxembourg.

Supplementary Materials: The following supporting information can be downloaded at: <https://www.mdpi.com/article/10.3390/app13137968/s1>, Video S1: Simulation video of the soft capture process. Software used: NVIDIA Omniverse.

Author Contributions: Conceptualization, M.H.D. and O.-O.C.-L.; Software, M.H.D. and O.-O.C.-L.; Validation, C.M.; Investigation, M.H.D. and O.-O.C.-L.; Data curation, M.H.D.; Writing—original draft, M.H.D. and O.-O.C.-L.; Writing—review & editing, M.H.D., O.-O.C.-L., B.C.Y., X.L. and C.M.; Supervision, M.O.-M. and C.M. All authors have read and agreed to the published version of the manuscript.

Funding: SnT-SpaceR has conducted this study under Luxembourg National Research Fund (FNR)—BRIDGES funding for “High fidelity tEsting eNvironment for Active Space Debris Removal—HELEN”, project ref: BRIDGES2021/MS/15836393, and FNR funding for “design of a Capturing, Absorbing, SEcuring system for active space Debris removal—CASED” project FNR16678722.

Institutional Review Board Statement: Not applicable.

Informed Consent Statement: Not applicable

Data Availability Statement: Restrictions apply to the availability of these data. Data was obtained from DISCOS (Database and Information System Characterising Objects in Space) and are available at <https://discosweb.esoc.esa.int/objects> with the permission of ESA.

Conflicts of Interest: The authors declare no conflict of interest.

Appendix A

More detailed visualisation of the data of Figure 16 is provided for each contact time in the range of [4–12] s in Figures A1–A4 and 20. Based on the derived diagrams, the desired stiffness and damping coefficients of the hybrid system’s equivalent compliance can be selected for a specific debris mass and minimum contact time required.

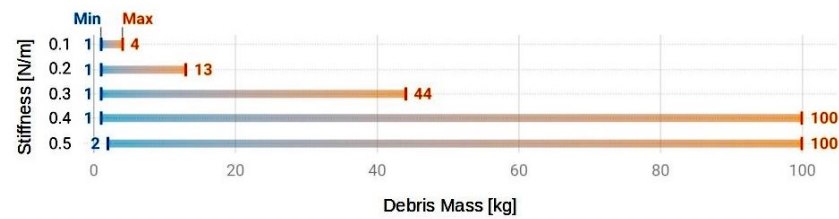


Figure A1. Range of space debris to be targeted for 4 s contact time.

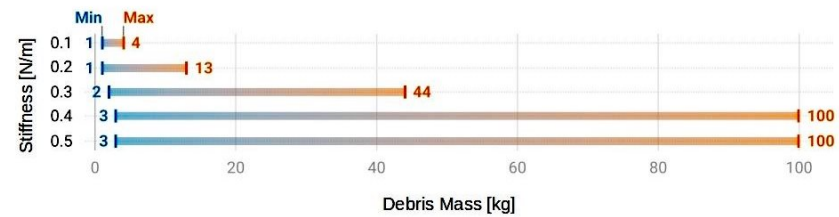


Figure A2. Range of space debris to be targeted for 6 s contact time.

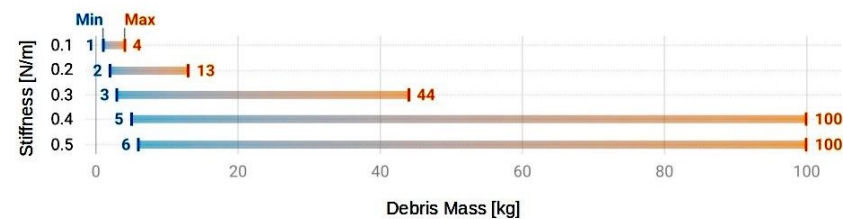


Figure A3. Range of space debris to be targeted for 8 s contact time.

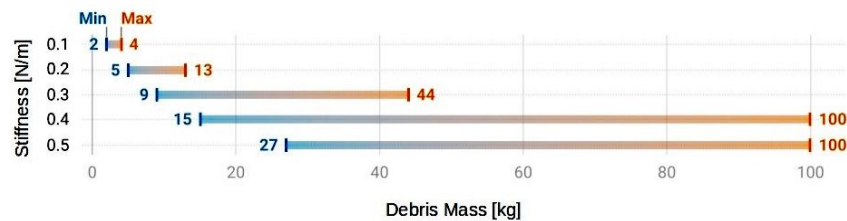


Figure A4. Range of space debris to be targeted for 12 s contact time.

References

- Bernhard, P.; Deschamps, M.; Zaccour, G. Large satellite constellations and space debris: Exploratory analysis of strategic management of the space commons. *Eur. J. Oper. Res.* **2023**, *304*, 1140–1157. [\[CrossRef\]](#)
- Space Environment Statistics. Available online: <https://sdup.esoc.esa.int/discosweb/statistics/> (accessed on 15 September 2022).
- Drmola, J.; Hubik, T. Kessler Syndrome: System Dynamics Model. *Space Policy* **2018**, *44–45*, 29–39. [\[CrossRef\]](#)
- Liou, J.C. Active Debris Removal and the Challenges for Environment Remediation. In Proceedings of the 28th International Symposium on Space Technology, Ginowan, Japan, 29 August–2 September 2012.
- Aslanov, V.; Ledkov, A. 2—Space Debris Problem. In *Attitude Dynamics and Control of Space Debris During Ion Beam Transportation*; Springer: Berlin, Germany, 2023. [\[CrossRef\]](#)
- Bonnal, C. Active debris removal Recent progress and current trends. *Acta Astronaut.* **2013**, *85*, 51–60. [\[CrossRef\]](#)
- Borelli, G.; Gaias, G.; Colombo, C. Rendezvous and proximity operations design of an active debris removal service to a large constellation fleet. *Acta Astronaut.* **2023**, *205*, 33–46. [\[CrossRef\]](#)
- Færgestad, R.; Holmen, J.; Berstad, T.; Cardone, T.; Ford, K.; Børvik, T. Coupled finite element-discrete element method (FEM/DEM) for modelling hypervelocity impacts. *Acta Astronaut.* **2023**, *203*, 296–307. [\[CrossRef\]](#)
- Yalçın, B.C.; Martinez, C.; Delisle, M.H.; Rodriguez, G.; Zheng, J.; Olivares-Mendez, M. ET-Class: An Energy Transfer-Based Classification of Space Debris Removal Methods and Missions. *Front. Space Technol.* **2022**, *3*, 23. [\[CrossRef\]](#)
- Liu, J.; Cui, N.; Shen, F.; Rong, S. Dynamics of Robotic Geostationary orbit Restorer system during deorbiting. *IEEE Aerosp. Electron. Syst. Mag.* **2014**, *29*, 36–42. [\[CrossRef\]](#)

11. Fang, G.; Zhang, Y.; Sun, Y.; Huang, P. On the Stiffness Selection for Tethered Space Robot. In Proceedings of the 2022 IEEE International Conference on Robotics and Biomimetics (ROBIO), Xishuangbanna, China, 5–9 December 2022; pp. 297–302. [[CrossRef](#)]
12. Wu, S.; Mou, F.; Liu, Q.; Cheng, J. Contact dynamics and control of a space robot capturing a tumbling object. *Acta Astronaut.* **2018**, *151*, 532–542. [[CrossRef](#)]
13. Nishida, S.I.; Uenaka, D.; Matsumoto, R.; Nakatani, S. Lightweight Robot Arm for Capturing Large Space Debris. *J. Electr. Eng.* **2018**, *6*, 271–280. [[CrossRef](#)]
14. Somov, Y.; Butyrin, S.; Somov, S. Guidance and Control of a Space Robot-manipulator at Approach and Capturing a Passive Satellite. *IFAC-PapersOnLine* **2019**, *52*, 538–543. [[CrossRef](#)]
15. Yan, L.; Xu, W.; Hu, Z.; Liang, B. Multi-objective configuration optimization for coordinated capture of dual-arm space robot. *Acta Astronaut.* **2020**, *167*, 189–200. [[CrossRef](#)]
16. Liu, Z.; Lin, T.; Wang, H.; Yue, C.; Cao, X. Design and Demonstration for an Air-bearing-based Space Robot Testbed. In Proceedings of the 2022 IEEE International Conference on Robotics and Biomimetics (ROBIO), Samui, Thailand, 4–9 December 2022; pp. 321–326. [[CrossRef](#)]
17. Wang, X.; Shi, L.; Katupitiya, J. A strategy to decelerate and capture a spinning object by a dual-arm space robot. *Aerosp. Sci. Technol.* **2021**, *113*, 106682. [[CrossRef](#)]
18. Chen, G.; Wang, Y.; Wang, Y.; Liang, J.; Zhang, L.; Pan, G. Detumbling strategy based on friction control of dual-arm space robot for capturing tumbling target. *Chin. J. Aeronaut.* **2020**, *33*, 1093–1106. [[CrossRef](#)]
19. Cao, Y.; Wang, S.; Zheng, X.; Ma, W.; Xie, X.; Liu, L. Reinforcement learning with prior policy guidance for motion planning of dual-arm free-floating space robot. *Aerosp. Sci. Technol.* **2023**, *136*, 108098. [[CrossRef](#)]
20. Sze, H.Y.; Chhabra, R. Trajectory Generation for Space Manipulators Capturing Moving Targets Using Transfer Learning. In Proceedings of the 2023 IEEE Aerospace Conference, Big Sky, MT, USA, 4–11 March 2023. [[CrossRef](#)]
21. Psomiadis, E.; Papadopoulos, E. Model-Based/Model Predictive Control Design for Free Floating Space Manipulator Systems. In Proceedings of the 2022 30th Mediterranean Conference on Control and Automation (MED), Athens, Greece, 28 June–1 July 2022; pp. 847–852. [[CrossRef](#)]
22. Fauré, M.; Henry, D.; Cieslak, J.; Colmenarejo, P.; Ankersen, F. A H_{∞} control solution for space debris removal missions using robotic arms: The ESA e.Deorbit case. In Proceedings of the 2022 UKACC 13th International Conference on Control (CONTROL), Plymouth, UK, 20–22 April 2022; pp. 122–129. [[CrossRef](#)]
23. Kayastha, S.; Katupitiya, J.; Pearce, G.; Rao, A. Comparative study of post-impact motion control of a flexible arm space robot. *Eur. J. Control* **2023**, *69*, 100738. [[CrossRef](#)]
24. Viscuso, S.; Gualandris, S.; De Ceglia, G.; Visentin, V. Chapter 18—Shape memory alloys for space applications. In *Shape Memory Alloy Engineering*, 2nd ed.; Concilio, A., Antonucci, V., Auricchio, F., Lecce, L., Sacco, E., Eds.; Butterworth-Heinemann: Boston, MA, USA, 2021; pp. 609–623. [[CrossRef](#)]
25. Sinatra, N.R.; Teeple, C.B.; Vogt, D.M.; Parker, K.K.; Gruber, D.F.; Wood, R.J. Ultragentle manipulation of delicate structures using a soft robotic gripper. *Sci. Robot.* **2019**, *4*, eaax5425. [[CrossRef](#)]
26. Li, X.; Chen, Z.; Wang, Y. Detumbling a Space Target Using Soft Robotic Manipulators. In Proceedings of the 2022 IEEE International Conference on Mechatronics and Automation (ICMA), Guilin, China, 7–10 August 2022; pp. 1807–1812. [[CrossRef](#)]
27. Wang, W.; Tang, Y.; Li, C. Controlling bending deformation of a shape memory alloy-based soft planar gripper to grip deformable objects. *Int. J. Mech. Sci.* **2021**, *193*, 106181. [[CrossRef](#)]
28. Lu, Y.; Xie, Z.; Wang, J.; Yue, H.; Wu, M.; Liu, Y. A novel design of a parallel gripper actuated by a large-stroke shape memory alloy actuator. *Int. J. Mech. Sci.* **2019**, *159*, 74–80. [[CrossRef](#)]
29. Feng, L.; Martinez, P.; Dropmann, M.; Ehresmann, M.; Ginsberg, S.; Herdrich, G.; Laufer, R. MEDUSA—Mechanism for Entrapment of Debris Using Shape memory Alloy. In Proceedings of the 1st ESA NEO and Debris Detection Conference, Darmstadt, Germany, 22–24 January 2019.
30. Jiang, H.; Hawkes, E.W.; Fuller, C.; Estrada, M.A.; Suresh, S.A.; Abcouwer, N.; Han, A.K.; Wang, S.; Ploch, C.J.; Parness, A.; et al. A robotic device using gecko-inspired adhesives can grasp and manipulate large objects in microgravity. *Sci. Robot.* **2017**, *2*, eaan4545. [[CrossRef](#)] [[PubMed](#)]
31. Hashizume, J.; Huh, T.M.; Suresh, S.A.; Cutkosky, M.R. Capacitive Sensing for a Gripper with Gecko-Inspired Adhesive Film. *IEEE Robot. Autom. Lett.* **2019**, *4*, 677–683. [[CrossRef](#)]
32. Estrada, M.A.; Hockman, B.; Bylard, A.; Hawkes, E.W.; Cutkosky, M.R.; Pavone, M. Free-Flyer Acquisition of Spinning Objects with Gecko-Inspired Adhesives. In Proceedings of the 2016 IEEE International Conference on Robotics and Automation (ICRA), Stockholm, Sweden, 16–21 May 2016. [[CrossRef](#)]
33. Su, Y.; Hou, X.; Li, L.; Cao, G.; Chen, X.; Jin, T.; Jiang, S.; Li, M. Study on impact energy absorption and adhesion of biomimetic buffer system for space robots. *Adv. Space Res.* **2020**, *65*, 1353–1366. [[CrossRef](#)]
34. Mitros, Z.; Rekleitis, G.; Papadopoulos, E. Impedance control design for on-orbit docking using an analytical and experimental approach. In Proceedings of the 2017 25th Mediterranean Conference on Control and Automation (MED), Valletta, Malta, 3–6 July 2017; pp. 1244–1249. [[CrossRef](#)]
35. Zhang, G.; Zhang, Q.; Feng, Z.; Chen, Q.; Yang, T. Dynamic modeling and simulation of a novel mechanism for adhesive capture of space debris. *Adv. Space Res.* **2021**, *68*, 3859–3874. [[CrossRef](#)]

36. Moosavian, S.A.A.; Papadopoulos, E. Multiple impedance control for object manipulation. In Proceedings of the 1998 IEEE/RSJ International Conference on Intelligent Robots and Systems Innovations in Theory, Practice and Applications (Cat. No. 98CH36190), Victoria, BC, Canada, 13–17 October 1998; Volume 1, pp. 461–466.
37. Hogan, N. Impedance control: An approach to manipulation. In Proceedings of the 1984 American Control Conference IEEE, San Diego, CA, USA, 6–8 June 1984; pp. 304–313.
38. Koga, K.; Fukui, Y. Deorbiting of Satellites by a Free-Flying Space Robot by Combining Positioning Control and Impedance Control. In Proceedings of the 2022 22nd International Conference on Control, Automation and Systems (ICCAS), Jeju, Republic of Korea, 27 November–1 December 2022; pp. 965–971. [[CrossRef](#)]
39. ClearSpace. Available online: <https://clearspace.today/> (accessed on 15 September 2022).
40. Biesbroek, R.; Aziz, S.; Wolahan, A.; Cipolla, S.; Richard-Noca, M.; Piguët, L. The clearspace-1 mission: ESA and clearspace team up to remove debris. In Proceedings of the European Conference on Space Debris (Virtual), Darmstadt, Germany, 20–23 April 2021.
41. DiscoWeb. Available online: <https://discosweb.esoc.esa.int/objects> (accessed on 15 September 2022).
42. ESA Space Debris Mitigation WG. *ESA Space Debris Mitigation Compliance Verification Guidelines*; European Space Agency: Paris, France, 2015.
43. Hawkes, E.W.; Jiang, H.; Cutkosky, M.R. Three-dimensional dynamic surface grasping with dry adhesion. *Int. J. Robot. Res.* **2015**, *35*, 943–958. [[CrossRef](#)]
44. Suresh, S. Engineering Gecko-Inspired Adhesives. 2020. Available online: <https://phowpublished.stanford.edu/cp134gr3166> (accessed on 15 September 2022).
45. Fehse, W. *Automated Rendezvous and Docking of Spacecraft*; Cambridge University Press: Cambridge, UK, 2003; Volume 16.
46. Brannan, J.; Scott, N.; Carignan, C. Robot Servicer Interaction with a Satellite During Capture. In Proceedings of the International Symposium on Artificial Intelligence, Robotics and Automation in Space (iSAIRAS), Madrid, Spain, 4–6 June 2018.
47. Stronge, W.J. *Impact Mechanics*; Cambridge University Press: Cambridge, UK, 2018.
48. Mitros, Z.; Paraskevas, I.S.; Papadopoulos, E.G. On robotic impact docking for on orbit servicing. In Proceedings of the 2016 24th Mediterranean Conference on Control and Automation (MED) IEEE, Athens, Greece, 21–24 June 2016; pp. 1120–1125.
49. Nanos, K.; Xydi-Chrysafi, F.; Papadopoulos, E. On impact de-orbiting for satellites using a prescribed impedance behavior. In Proceedings of the 2019 IEEE 58th Conference on Decision and Control (CDC) IEEE, Nice, France, 11–13 December 2019; pp. 2126–2131.

Disclaimer/Publisher’s Note: The statements, opinions and data contained in all publications are solely those of the individual author(s) and contributor(s) and not of MDPI and/or the editor(s). MDPI and/or the editor(s) disclaim responsibility for any injury to people or property resulting from any ideas, methods, instructions or products referred to in the content.